CHALMERS
UNIVERSITY OF TECHNOLOGY

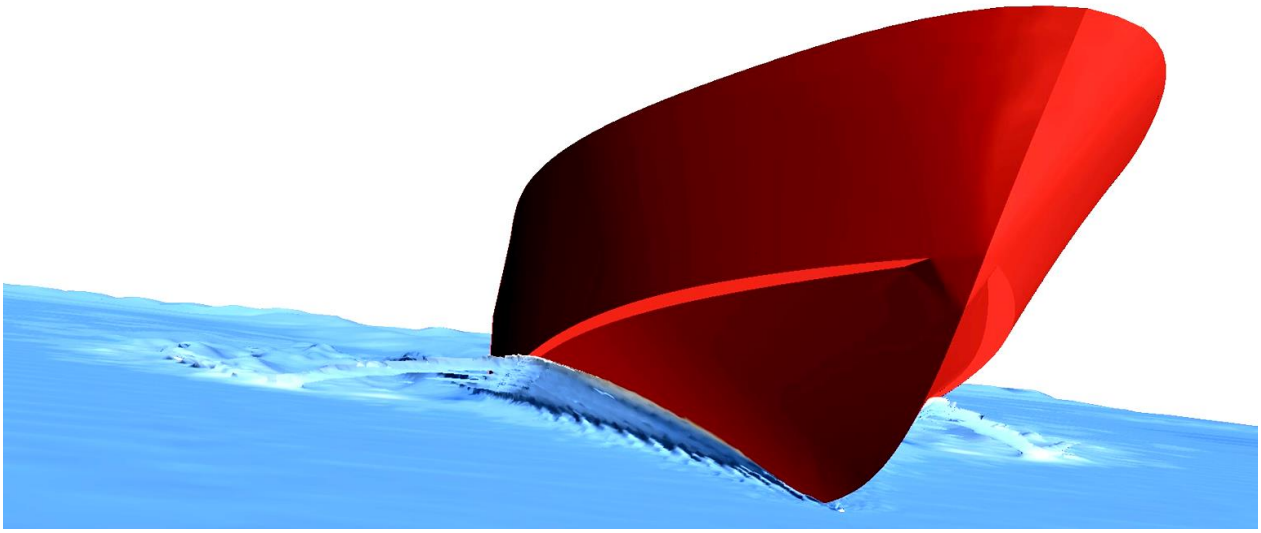

Systematic variations of parameters affecting waterjet-hull interaction

Master's thesis in Naval Architecture and Ocean Engineering

JOHAN ANDERSEN
GUSTAV MOE

Department of Shipping and Marine Technology
CHALMERS UNIVERSITY OF TECHNOLOGY
Gothenburg, Sweden 2014
Report No. X-14/301

A THESIS FOR THE DEGREE OF MASTER OF SCIENCE

Systematic variations of parameters affecting waterjet-hull interaction

JOHAN ANDERSEN
GUSTAV MOE

Department of Shipping and Marine Technology
CHALMERS UNIVERSITY OF TECHNOLOGY
Gothenburg, Sweden 2014

Systematic variations of parameters affecting waterjet-hull interaction

JOHAN ANDERSEN
GUSTAV MOE

Report No. X-14/301

Department of Shipping and Marine Technology
Chalmers University of Technology
SE-412 96 Gothenburg
Sweden
Telephone +46 (0)31-772 1000

Printed by Chalmers Reproservice
Gothenburg, Sweden, 2014

Systematic variations of parameters affecting waterjet-hull interaction

JOHAN ANDERSEN

GUSTAV MOE

Department of Shipping and Marine Technology

Chalmers University of Technology

Abstract

The purpose of this thesis is to follow a methodology in which computational models with two degrees of freedom (2DOF), based on the finite volume method, are validated and used to investigate how certain phenomena and parameters, especially the longitudinal position of the waterjet intake, affect resistance and thrust deduction (t) for the STREAMLINE hull. To arrive at a scientific answer to this question a methodology is carried out comprised of a grid dependence study followed by three studies of systematic variation. These include variation of Froude number, variation of initial trim (LCG) and variation of waterjet intake positions. Comparing the output from the Froude number variation and initial trim studies with towing tank test data, error trends are found and are used to obtain the reliability of the computational models. These error trends can then give an indication of the validity of the results from the variation of waterjet intake position study.

The results from the grid dependence study show an effective mesh size for the bare hull model of around 2.6 million elements. By applying this effective mesh size to the BH model, the error trends from the different parameter studies are obtained. The bare hull trends obtained from the Froude number and trim variation studies converge to an error span between 6-8%. A similar validation process using error trends for self propulsion has not been possible due to a lack of model test data. However, with the four model test data points available, it seems that the self propulsion model is reliable within at least a Froude number span of 0.44-0.48.

It is found that the effect of varying the Froude number for four degrees bow up initial trim and 2DOF is similar to the effect of varying the Froude number for a zero degree initial trim with a fixed hull. It is also found that the simulated resistance peak for BH appears at a lower Froude number than the measured resistance peak for BH. Also, the SP resistance peak appears before the BH resistance peak. In all tested cases, the resistance peaks are found to be correlated with the transom clearance phenomena. The trim variation study shows that the optimum initial trim for the STREAMLINE hull at design speed (Fn = 0.996) is the even keel trim for both BH and SP. The position variation study shows that the optimum longitudinal position for the center of the waterjet intake is 465 mm fore of the transom. This study also shows that the difference in resistance between the best and worst position for each Froude number differs with about 2-6%.

These results are a good start in gaining knowledge about waterjet-hull interaction and how waterjets can be delivered and installed to improve performance and sustainability.

Keywords: waterjet, STARCCM+, STREAMLINE, 2DOF, finite volume method, waterjet-hull interaction, net thrust, thrust deduction, hull efficiency

Sammanfattning

Målet med uppsatsen är att följa en metodik där beräkningsmodeller för två frihetsgrader baserade på finita volymsmetoden valideras och används för att undersöka hur vissa fenomen och parametrar, i synnerhet den longitudinella placeringen av ett vattenjetintag, påverkar motstånd och thrust deduction för STREAMLINE skrovet. För att komma fram till ett vetenskapligt svar på frågeställningen följs en metodik som omfattar en nätstudie följt av tre parameterstudier för Froudenummer, initialt trim, och intagsposition. Genom att jämföra utdatan från de två förstnämnda parameterstudierna med modelltestdata så hittas feltrender som används för att bestämma pålitligheten av beräkningsmodellerna. Dessa feltrender används sedan för att validera resultaten från variationen av intagspositionerna.

Resultaten från nätstudien visar en effektiv nätstorlek för bare hull modellen på ungefär 2,6 miljoner element som sedan används i parameterstudierna för bare hull. Studierna för Froudenummervariation och initial trimvariation resulterar i felmarginaler på 6-8%. En lika grundlig validering med feltrender för självdriftsmodellen har inte varit möjlig på grund av brist på modelltestdata för självdrift, men med de fyra tillgängliga datapunkterna verkar det som att självdriftsmodellen är pålitlig i åtminstone Froudenummerspannet 0.44-0.48.

Resultatet från variationen av Froudenummer för fyra graders initialt trim och två frihetsgrader visar samma effekt som för noll graders initialt trim med fixerat skrov. Det visar sig även i detta fall att motståndspeaken för bare hull simuleringarna inträffar vid ett lägre Froudenummer än den uppmätta motståndspeaken för bare hull. Dessutom kommer motståndspeaken för självdrift vid ett lägre Froudenummer än för bare hull. För både bare hull och självdrift visar det sig att peaken och akterspegelstömningen sammanfaller. Trimvariationsstudierna visar att det mest optimala initiala trimmet för STREAMLINE skrovet vid design Froudenummer (Fn=0,996) är vid initialt trim noll för bare hull och självdrift. Positionvariationsstudien visar att den optimala longitudinella positionen för vattenjetintagets centrum är 465 mm för om akterspegeln. Studierna visar även att skillnaden i motstånd mellan bästa och sämsta positionen för varje Froudenummer är ungefär 2-6%.

Dessa resultat är en bra början i att få ökade kunskaper för hur vattenjet-skrov interaktionen fungerar och hur vattenjetaggregat kan levereras och installeras för att förbättra prestanda och hållbarhet.

Nyckelord: vattenjet, STARCCM+, STREAMLINE, 2DOF, finita volymsmetoden, vattenjet-skrov interaktion, net thrust, thrust deduction, skroveffektivitet.

Preface

This thesis is a part of the requirements for the master's degree at Chalmers University of Technology, Göteborg, and has been carried out at the Division of Marine Design, Department of Shipping and Marine Technology, Chalmers University of Technology.

First and foremost we would like to express our gratitude to our examiner and supervisor Professor Rickard Bensow at the Department of Shipping and Marine Technology for supporting us with valuable insight and assistance. We would also like to thank Professor Lars Larsson and Ph.D student Arash Eslamdoost for valuable discussions and supervision throughout the project.

Furthermore we would like to extend our appreciation to Marko Hyensjö and Rickard Gustavsson at Rolls-Royce for the assistance during the time we spent in Kristinehamn learning valuable tools for continuing our project. Finally, we thank Per Österdahl at CD-adapco for assisting us with licensing of STARCCM+ throughout the project.

Göteborg, June, 2014
Johan Andersen & Gustav Moe

Abbreviations

BH : Bare hull
SP : Self propulsion
Fn : Froude number
2DOF : two degrees of freedom
LCG : Longitudinal center of gravity
Pos : Position
CPU : Central processing unit

Nomenclature

R_{bh} : Bare hull resistance
T_g : Gross thrust
t : Thrust deduction
η_H : Total hull efficiency
w : Wave fraction
t_r : Thrust deduction fraction
t_j : Jet system thrust deduction
T_{net} : Net thrust vector component
C_T : Total resistance coefficient
C_{Tbh} : Total resistance coefficient for BH
C_{Tsp} : Total resistance coefficient for SP
ρ : Water density
S_w : Wetted surface
v : Hull velocity
E : Error
S : Fluid flow solution
U_{val} : Validation uncertainty span
U_{SN} : Numerical uncertainty
U_I : Iterative uncertainty
U_G : Discretization uncertainty
S_g : Grid discretization error
h_i : Grid spacing
S_i : Solution of the i:th grid
S_0 : Extrapolated solution to zero step size
α : Constant
P : Order of accuracy
$H.O.T$: Higher order terms
δ_{RE} : Richardson extrapolation error
r : Grid refinement ratio
ε : Difference between computed solutions
R : Convergence ratio
U_{SD} : Standard deviations
U_D : Experimental uncertainty
D : Pump outlet diameter
y^+ : Non-dimensionalized length

Table of contents

1. Introduction

This project is initiated and defined by Rolls Royce in cooperation with Chalmers in order to investigate and gain a better understanding of waterjet-hull interaction, and more specifically the effect of the longitudinal positioning of the waterjet intake. Understanding this can potentially lead to a better interface between waterjets and hulls in order to minimize fuel consumption and increase sustainability.

The first chapter includes a short description of the features and functions of today's waterjet units. Previous studies related to the interaction between waterjet units and ship hulls are then discussed. These studies include the STREAMLINE project with SSPA towing tank tests and parts of a PhD licentiate thesis with an additional paper. A gap in previous studies are shown and discussed which lead to the scope of the project and its delimitations.

1.1. Features and functions of waterjet units

A waterjet is much like the turbojet of an aircraft with the main difference being the fluid in which it operates. The thrust force generated by the waterjet comes from adding momentum to the water by accelerating the flow through the inlet and expelling it sternward through the nozzle exit. The difference between the momentum exiting the nozzle and the momentum entering the inlet is called momentum flux. An impeller connected to the drive shaft draws water through the inlet channel adding head to the water and a stator removes the water swirl which redirects the flow so that a straight, high-speed jet is created. Steering is made possible either by horizontally rotating the nozzle or by deflecting the discharged jet with directional rudders. To enable stopping and reversing, a reversing bucket is lowered over the nozzle exit to switch the direction of the thrust force.

Waterjets are mostly used for military vessels and ferries with high speed and maneuverability demands as they in general have higher efficiencies at higher speeds. Configurations can generally include up to three waterjets. In the case of three waterjets, the one in the center is called booster and only supplies the vessel with additional thrust without maneuverability capability. The power range of waterjets spans from around 0.1 - 40MW with pump diameters ranging from approximately 30 - 200 centimeters.

When measuring thrust of a vessel with a conventional propeller, the net thrust is used. The net thrust is the measured force transmitted via the propeller shaft to the propeller. For a waterjet, the net thrust is affected by both the impeller shaft and the ducting channel. Measuring the net thrust for a waterjet is therefore very hard and complicated. To solve this problem, the gross thrust T_g is introduced. The gross thrust is the horizontal force vector evolved from the exiting momentum flux in the nozzle. When attaching a waterjet on a hull the total efficiency of the vessel will change. To measure and compare this difference, a total thrust deduction (t) is introduced which describes the connection between the BH resistance R_{bh} and the gross thrust T_g.

$$T_g(1-t) = R_{bh} \tag{1}$$

The decrease in thrust deduction (t) corresponds to an increased total hull efficiency (η_H) according to Equation 2 (Schneekluth & Bertram V, 1998) where *w* is the wake fraction.

$$\eta_H = \frac{1-t}{1-w} \tag{2}$$

The total thrust deduction can be simplified as the sum of a jet system thrust deduction t_j and a thrust deduction fraction t_r.

$$t = t_r + t_j \tag{3}$$

The introduced jet system thrust deduction t_j is normally very small and hard to measure due to technical issues. Therefore Equation 4 is used instead of Equation 1 where T_{net} is the horizontal component of the net thrust vector (Eslamdoost, 2012).

$$T_{net}(1 - t_r) = R_{bh} \tag{4}$$

In this study T_{net} and t_r are the resulting data for SP simulations. The resistance for BH and T_{net} for SP is transformed to a non-dimensional resistance coefficient (C_T) according to Equation 5, to be used for comparison in some cases throughout the report (Larsson & Raven, 2010).

$$C_{Tbh} = \frac{2R_{bh}}{\rho S_w v^2} \quad or \quad C_{Tsp} = \frac{2T_{net}}{\rho S_w v^2} \tag{5}$$

Here ρ is the water density, S_w the wetted surface of the hull and v the hull velocity.

1.2. Significant work

There has been an EU FP7 research project regarding propulsion systems called the STREAMLINE Project. Three of the many partners in this project are SSPA, Rolls-Royce and Chalmers University of Technology. SSPA have carried out design work, analyses and model testing of waterjets and other propulsors. They have also designed a hull specifically developed for these tests with extensive data from BH and SP tests. We will refer to this as the STREAMLINE hull and its particulars are shown in Table 1. Chalmers hosts the Rolls-Royce University Technology Centre (UTC) in Computational Hydrodynamics. In their cooperation, they have sponsored several projects within this area.

Table 1 Particulars for the STREAMLINE hull

STREAMLINE particulars	
Scale factor	7.5
LPP (model)	2.27 m
Beam (model)	0.62 m
Design Fn	1

Arash Eslamdoost, a PhD student from Chalmers involved in the Rolls-Royce University Technology Centre, has been developing a computational method to investigate the interaction between the waterjet unit and hull (Eslamdoost, 2012). His work is initiated and completely financed by Rolls-Royce Marine AB within the UTC cooperation. In his doctoral thesis he tries to find a link between the net thrust and the gross thrust of a waterjet unit. This

is done in two steps. In the first step he creates an iterative algorithm for modeling the effect of the waterjet on the hull called the pressure jump method. This potential flow method is validated by comparing the computational results to experimental data. The second step is an investigation of how certain parameters influence the thrust deduction of a waterjet propelled vessel by employing the pressure jump method. We here cite the main conclusions from his licentiate thesis (Eslamdoost, 2012):

1. There is no sinkage or trim for a waterjet in free-stream conditions, i.e. for a waterjet fitted to an infinitely large flat plate and ejecting the flow horizontally. This is under the condition of infinitely deep water.
2. The waterjet induced pressure on the hull increases the sinkage, which increases resistance.
3. The influence of the waterjet-induced pressure on the trimming moment depends on the distance between the waterjet intake and the transom, and on the position of the centre of floatation. For most hulls a bow-down moment is generated, but if the intake is far aft, a moment in the other direction may be generated. Also, if the hull is very long, with a centre of floatation at a large distance from the intake, the moment may be bow-up.
4. An inclination of the waterjet nozzle always induces a bow-down effect, as does the resistance/thrust couple.
5. There is an optimum trim angle for the hull where the resistance is minimum. This is normally obtained where the transom has an optimum size. An increased trim may increase or decrease the resistance depending on the position on the resistance/trim curve relative to the optimum trim angle. The trim angle is one candidate for reducing the resistance, unless the hull has been optimized for self-propulsion.
6. Wave resistance normally increases due to deepening of wave trough at the stern.
7. The transom clearance is influenced by the waterjet in two ways: the critical Froude number for transom clearance is increased and the splashing of the waterjet into the stern wave may (partly) fill the trough behind the transom, thus decreasing the transom resistance. The transom clearance effect is the other important factor that may reduce resistance and cause a negative thrust deduction.
8. The viscous resistance decreases due to the missing surface covering the intake opening, but it may increase somewhat due to the changes in the boundary layer around the intake.

A paper following this thesis called *Waterjet Propelled Hull Transom Clearance* (Eslamdoost, et al., 2013) gives a more thorough investigation of the transom clearance phenomena by accounting for the viscous effects in an investigation using STARCCM+. There are two main conclusions drawn from this paper. The first conclusion is that the correspondence between measured BH and simulated BH data is better for Froude numbers after the measured resistance peak. The second conclusion from his paper is that there is a difference in resistance peak between SP and BH for even keel trim and that the resistance peak corresponds to the transom clearance.

The paper specifies three effects that may result in an early clearance of the waterjet driven hull transom. The first is the high momentum jet which pushes back the water behind the transom. The second effect is that the trailing waves are less prone to breaking due to that the

hull boundary layer at the transom is thinner because of the high momentum jet. The third effect is that the waves are lower beside the hull and therefore will not break inwards and fill the hollow as easily due to the suction of the intake. The three effects result in an early clearance of the waterjet driven hull transom compared to BH transom clearance.

The Froude number at which transom clearance occurs is called the critical Froude number, not to be confused with the critical Froude number for shallow water. In the low Froude number range the resistance of the self propelled hull is higher than the BH resistance. However, the difference in resistance rapidly decreases when approaching the critical Froude number. Figure 1 shows the comparison between the total resistance coefficient (C_T) for BH and SP hull before and after the resistance peak as found in his paper.

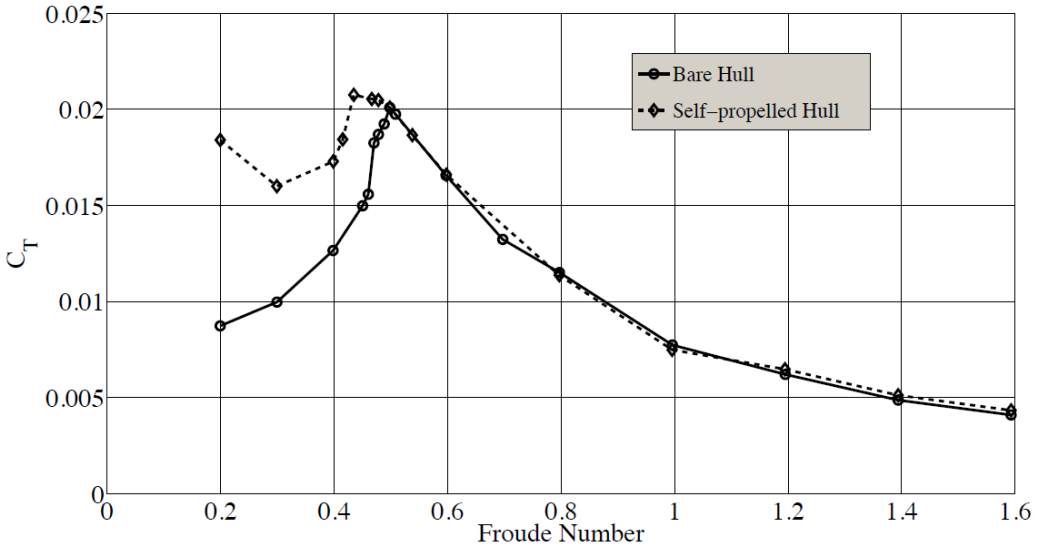

Figure 1 A comparison between the total resistance coefficient for BH and SP for fixed sinkage and trim **(Eslamdoost, et al., 2013)**.

1.3. Gap in previous work

The scope of this thesis work is defined by some gaps identified in the work performed at Chalmers to date. The list can of course be made much longer but the main issues addressed in this work is described below.

A grid dependence study has mainly been done for high Froude numbers. It should also be done for low Froude numbers because lower speeds generally require a finer mesh resolution due to a higher wave frequency along the hull. Each wave along the hull needs to be represented by a certain amount of cells to give a good representation.

The Froude number variation studies have been performed for fixed sinkage and trim at even keel for BH and SP. This has not been done for free sinkage and trim or other initial trims. Therefore, the Froude number variation study should be performed for free sinkage and trim, for an extreme initial trim to see the effects on resistance peak and transom clearance.

Simulations or towing tank tests have not been performed for variations of the waterjet intake positioning. Therefore there is no found correlation between waterjet intake positioning and

thrust deduction. A waterjet intake variation study would be interesting for Rolls Royce in order to find the affects of the intakes location on efficiency and sustainability.

1.4. Purpose

The purpose of this thesis is to follow a methodology in which computational models with two degrees of freedom (2DOF), based on the finite volume method, are validated and used to investigate how certain phenomena and parameters, especially the longitudinal position of the waterjet intake, affect resistance and thrust deduction (t) for the STREAMLINE hull. The phenomena and parameters investigated are transom clearance, velocity, initial trim, and the longitudinal position of the waterjet intake.

Thrust deduction describes the difference in resistance between BH and SP and by varying one parameter at a time the isolated effects of each parameter on thrust deduction can be investigated. The three parameters investigated in this study are just a few of the many different parameters that can potentially be studied, and it is done for one hull. Even so, answering this question is a good start to helping Rolls-Royce gain knowledge about how they can deliver and install their line of waterjets to improve the performance and sustainability for their clients.

A methodology is carried out comprised of a grid dependence study followed by three studies of systematic variation which include variation of Froude number, variation of initial trim (LCG) and variation of waterjet intake positions. Comparing the output from the Froude number variation and initial trim studies with towing tank test data, error trends are found and used to obtain the reliability of the computational models. These trends also give an indication of the validity of the results from the variation of waterjet intake position study. A flow chart of the project is shown in Figure 2.

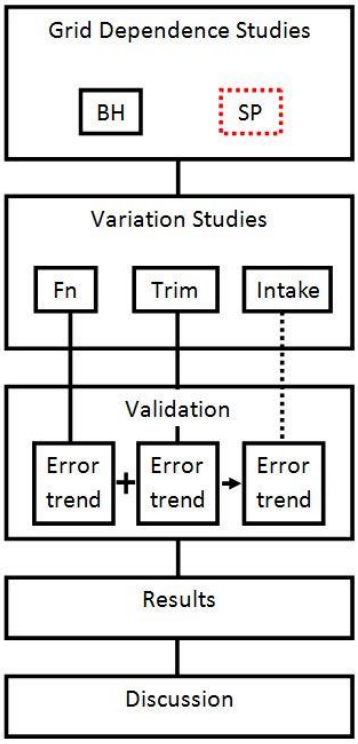

Figure 2 Flowchart over the work process for this project

1.5. Scope

The following Table 2 outlines the scope of the studies in this project. The process in which the studies are carried out and the specifics for each study is thoroughly explained in the methodology chapter.

Table 2 The scope of the project containing input and output for each study.

Study	Input	Output
Grid dependence study	- 6 mesh sizes btw 10^6- 10^7 cells - F_n = 0.398 - BH, fixed hull - Even keel	- Efficient mesh size for BH
Variation of Froude number	- 13 F_n around $F_{n,critical}$ for BH - 7 F_n around $F_{n,critical}$ for Self prop. - Initial trim (LCG)= Bow up (4˚) - Free sinkage & trim	- Resistance & T_{net} for BH & SP respectively at constant initial trim (LCG) - Trim data for SP - Thrust deduction fraction
Variation of initial trim	- F_n = 0.996 - Initial trim = 0.786˚, 0˚, -0.819˚, -1.693˚ - BH & SP - Free sinkage & trim	- Resistance & T_{net} for BH & SP respectively at constant F_n - Thrust deduction fraction
Variation of waterjet intake position	-Five intake positions -F_n=0.398, 0.498, 0.697, 0.996 -BH & SP -Even keel -Free sinkage & trim	- Resistance & T_{net} data for BH & SP respectively for varying F_n & waterjet intake position - Thrust deduction fraction
Validation	- Data from Variation of Froude number & initial trim studies - Data from SSPA tests - BH & SP	- Error trends

It is worth noting that the initial trim is defined as the trim at zero speed and is implemented by setting the longitudinal center of gravity (LCG) at the corresponding position along the hull. A negative trim angle is defined as a bow up trim, and a positive trim angle is defined as a bow down trim. Also, the five specific positions of the waterjet intake are specified and further explained in the methodology chapter.

2. Theory

The theory chapter describes a full validation process for two methods to estimate the numerical uncertainty: the factor of safety method and the least square root method. The chapter also briefly describes the different approaches used for turbulence modeling.

2.1. Validation

In order to certify that a numerical computation represents physical reality in a satisfying way one needs to know the level of accuracy of the representation and how one can track the errors that are inevitably introduced. Validation is the name given to the process of comparing the numerical fluid flow solution (S) with gathered test data (D) in order to find these errors (E). Through this process one can also quantify the magnitude of the errors to ensure that these fall within an acceptable range (U_{val}).

$$E = S - D \tag{6}$$

$$|E| \leq U_{val} \ (E \text{ is within the span of } U_{val})$$

A schematic of the validation process and an explanation of its steps are shown in Figure 3, referenced from *Ship resistance and flow from the Principle of Naval Architecture series* (Larsson & Raven, 2010).

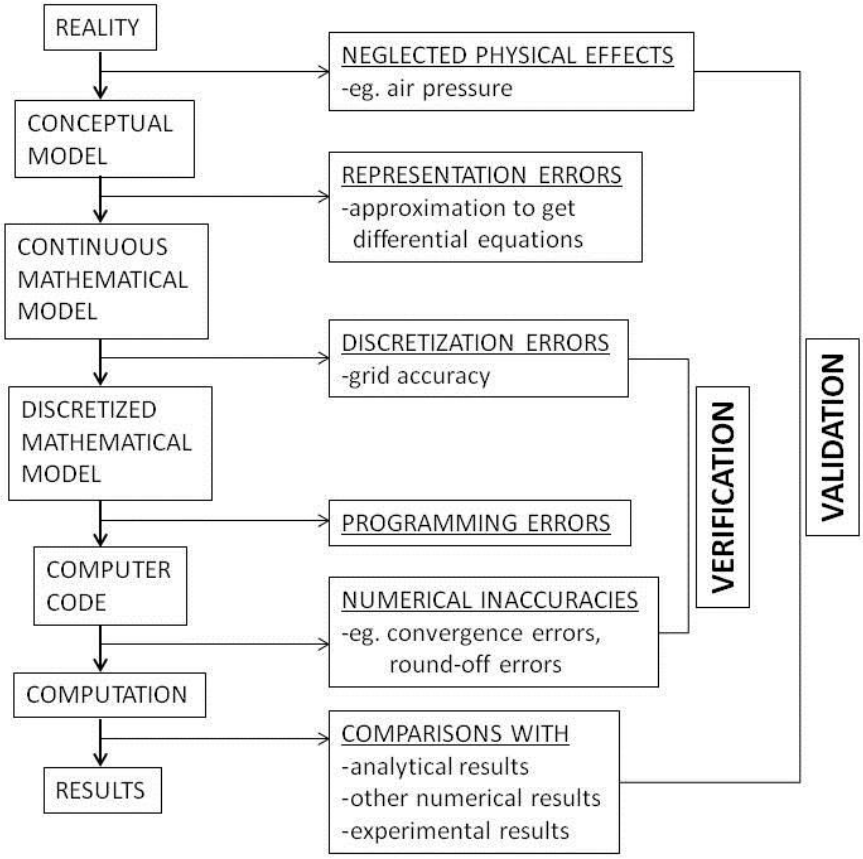

Figure 3 Sources of errors in computed results **(Larsson & Raven, 2010)**.

The first step in the modeling procedure is to create a conceptual model of the reality. Here, the important physical phenomena are identified and less important effects neglected. The contribution of errors from this step appears from the sum of neglected effects, for instance the flow around the above-water part of a ship etc.

The second step is to create a continuous mathematical model that translates the conceptual model into differential or integral equations. The errors from this step appear from the physical models introduced.

Step three is to create a discretized model which is an approximated version of the mathematical model. The discretized model contributes to the possibility of a numerical solution. Discretization errors are introduced due to the approximated representation of the continuous solution field.

The fourth step is to implement the discretized model in a computer code. This may cause errors like bugs and other programming errors. The result from the computer code also includes round off and iterative errors.

The errors from the first step to the last step are summed up to generate the total error. The part of the validation process that concerns discretization, convergence, programming and round-off errors is called verification and the corresponding numerical uncertainty is denoted by U_{SN}

$$U_{SN} = \sqrt{U_I^2 + U_G^2} \tag{7}$$

where U_I is the iterative uncertainty due to lack of convergence of the non-linear iterations and U_G is the discretization uncertainty.

Two methods of determining the numerical uncertainty are described in *CFD Predictions Including Verification and Validation of Hydrodynamic Forces and Moments on Ships in Restricted Waters* (Zou, 2012). The grid discretization uncertainty can be determined either by the Factor of Safety Method or the Least Square Root Method, both of which use Richardson Extrapolation. This technique assumes a structured grid so that the grid spacing (h_i) decreases equally in all directions. The grid discretization error (δ_g) is represented by:

$$\delta_g = S_i - S_0 = \alpha h_i^p + H.O.T \text{ (for } i\text{=1,2,3,4,…)} \tag{8}$$

where S_i is the solution of the i:th grid, S_0 is the extrapolated solution to the zero step size, α a constant and H.O.T is the higher order terms. When applying Richardson Extrapolation the factor p is adjusted to replace the higher order terms (H.O.T). Then the expression is simplified to

$$\delta_{RE} = S_i - S_0 = \alpha h_i^{p_{adj}} \tag{9}$$

2.1.1. Factor of safety method

The factor of safety method assumes that U_I is small compared to U_G. With increasing iterations the value for U_I decreases and with enough iterations the value of this uncertainty compared with the discretization uncertainty is negligible. Therefore

$$U_{SN} = U_G \tag{10}$$

A grid refinement ratio (r) is determined as the factor of decreasing grid spacing (h_i).

$$r = \frac{h_i}{h_{i-1}} \tag{11}$$

The corresponding computed solutions to the i:th grid are represented by S_i where ε is the difference between the computed solutions.

$$\varepsilon_{i,i-1} = S_i - S_{i-1} \tag{12}$$

This leads to the convergence ratio (R) defined as

$$R = \frac{\varepsilon_{i-2,i-1}}{\varepsilon_{i-1,i}} \tag{13}$$

If the convergence ratio falls in the span of monotonic convergence ($0<R<1$) the Richardson extrapolation is a valid description of the series of higher order terms into one factor.

$$\delta_g \approx \delta_{RE}$$

The order of accuracy (p) is determined from Equation 9 above,

$$p = \frac{\ln\left(\frac{\varepsilon_{23}}{\varepsilon_{12}}\right)}{\ln(r)} \tag{14}$$

which enables the calculation of δ_{RE}.

$$\delta_{RE} = S_1 - S_0 = \frac{\varepsilon_{12}}{r^p - 1} \tag{15}$$

The numerical uncertainty (U_{SN}^{FS}) is determined through safety factors that are based on statistical analysis

$$U_{SN}^{FS} = F_s P|\delta_{RE}| = \begin{cases} (2{,}45 - 0{,}8P)|\delta_{RE}|, 0 < P \leq 1 \\ (16{,}4 - 14{,}8P)|\delta_{RE}|, \ P > 1 \end{cases} \tag{16}$$

where $P=p/2$.

2.1.2. Least Square Root Method

The Least Square Root Method (LSRM) uses a curve fit to determine the order of accuracy and the numerical error. The large scatter of numerical solutions means that in order for this method to work it needs to include more than three grid densities. Similarly to the Factor of Safety Method, the discretization error (ε_{RE}) in LSRM has a subscript RE, as it follows the general form from Richardson Extrapolation.

$$\varepsilon_{RE} \approx \delta_{RE} = S_i - S_0 = \alpha h_i^p \qquad for\ i = 1{,}2, \ldots n_g, \ \ n_g > 3 \tag{17}$$

The three unknowns in this expression, S_i, α and p are determined by more than three solutions, where the observed order of accuracy (p) can be estimated by the curve fit of the LSRM. A function of the three unknowns is introduced as

$$f(S_o, \alpha, p) = \sqrt{\sum_{i=1}^{n_g} \left(S_i - \left(S_0 + \alpha h_i^p\right)\right)^2} \tag{18}$$

The behavior of the function depends on which of the following convergence conditions it falls under.

1) Monotonic convergence: $p > 0$

2) Oscillatory convergence: $n_{ch} \geq INT\left({}^{n_g}/_{3}\right)$
$n_{ch} is\ the\ number\ of\ triplets\ with\ (S_{i+1} - S_i)(S_i - S_{i-1}) < 0$

3) Anomalous behavior: otherwise

The observed order of accuracy depends highly on the scatter of the numerical solutions and therefore largely affects the numerical error. Therefore, in the LSRM there are three alternative estimates to the numerical error which can be used instead of the general Richardson Extrapolation form. These are

$$\delta_{RE}^{02} = S_i - S_0 = \alpha_{02} h_i^2 \tag{19}$$

$$\delta_{RE}^{12} = S_i - S_0 = \alpha_{11} h_i + \alpha_{12} h_i^2 \tag{20}$$

$$\delta_{\Delta M} = \frac{\Delta M}{\frac{h_{ng}}{h_1} - 1}\ where\ \Delta M\ is\ the\ data\ range. \tag{21}$$

$$\Delta M = \max\left(\left|S_i - S_j\right|\right)\ i \geq 1,\ j \leq n_g,\ h_{ng} is\ the\ step\ size\ of\ the\ n_g{:}th\ grid \tag{22}$$

Which one of the estimates to use depends on the value of p and on the convergence condition as listed above. As follows, the convergence condition therefore determines the formulation of the numerical uncertainty (U_{SN}):

$$U_{SN} = F_S|\varepsilon_{RE}| \tag{23}$$

1) Monotonic convergence:

a. $0.95 \leq p \leq 2.05$: $U_{SN} = 1.25\delta_{RE} + U_{SD}$ (24)
b. $p \leq 0.95$: $U_{SN} = \min(1.25\delta_{RE} + U_{SD},\ 3\delta_{RE}^{12} + U_{SD}^{12})$ (25)
c. $p \geq 2.05$: $U_{SN} = \max(1.25\delta_{RE} + U_{SD},\ 3\delta_{RE}^{02} + U_{SD}^{02})$ (26)

2) Oscillatory convergence:

$$U_{SN} = 3\delta_{\Delta M} \tag{27}$$

3) Anomalous behavior:

$$U_{SN} = \min(3\delta_{\Delta M}, 3\delta_{RE}^{12} + U_{SD}^{12}) \quad where\ U_{SD}, U_{SD}^{02},\ U_{SD}^{12}\ are\ standard\ deviations \tag{28}$$

$$U_{SD} = \sqrt{\frac{\sum_{i=1}^{n_g}\left(S_i - (S_0 + \alpha h_i^p)\right)^2}{n_g - 3}} \tag{29}$$

2.1.3 Validation criteria

The span of validation uncertainty (U_{val}) consists of numerical (U_{SN}) and experimental uncertainty (U_D).

$$U_{val} = \sqrt{U_{SN}^2 + U_D^2} \tag{30}$$

Experimental uncertainties are very hard to determine due to many sources of error in the measuring and testing equipment. This value is hard to determine and most testing facilities are unwilling to share their own experimental uncertainty value.

The errors have to be within the span of the validation uncertainty in order to satisfy the validation criteria. If the errors are not within the validation uncertainty there is something wrong with the physical representation in the fundamental mathematical equations.

$$|E| \leq U_{val} \tag{31}$$

2.2. Turbulence modeling

Turbulence modeling is complex but significant in order to account for the effects of turbulence in hydrodynamics. Turbulence is characterized by random and chaotic three dimensional eddies. Compared to laminar flow, turbulence introduces increased energy dissipation, mixing heat transfer and drag. The turbulence closure problem as it is known in fluid dynamics is a problem that exists because in turbulence modeling there are fewer equations than unknowns when trying to predict turbulent flow. There are different methods resulting in different accuracies when simulating turbulence. The three that will be discussed are direct numerical solution, large eddy simulation and Reynolds averaged Navier-Stokes referenced from the webpage *comsol.com* (Frei, 2014). The governing equations in all three methods are the Navier-Stokes motion equations.

Direct numerical solution (DNS) is the only approach that avoids the closure problem because DNS uses the exact Navier-Stokes equations that govern the fluid. Since the cell size is much smaller than the smallest eddy in the flow, this method solves the equations for every cell in a mesh, accounting for all eddies. The problem with this is that even modeling simple flow is much too time consuming and CPU demanding for conventional use. Also, the sheer amount of data gathered from DNS simulations is too difficult to handle.

Large Eddy Simulation (LES) employs LES filters that dispels eddies smaller than a certain predefined size and uses sub-grid models to represent the filtered eddies. The filters are applied to Navier-Stokes equations and thereby eliminate the small scale solutions of the simulation. Only accounting for large scale motions therefore reduces computational time and cost. Even so, LES is still considered too expensive and time consuming to be applied on entire hull simulations.

The Reynolds Average Navier Stokes-method time averages the Navier-Stokes equations. This contributes to a more uncertain/averaged result compared to the other approaches but is still considered sufficient for most applications. All parts of this project use the CFD software STAR CCM+ as a tool for the numerical results and the turbulence modeling approach used is the RANS-method.

When looking at turbulent velocity profile of a flow across a plate there are four regions to be considered at different lengths from the wall. These regions are called the viscous sub-layer, buffer layer, turbulent region and the inviscid region shown in Figure 4. The viscous sub-layer is a thin laminar flow near the wall with a linear velocity profile. Directly after the viscous sub-layer the buffer region begins and is a transition to turbulent flow.

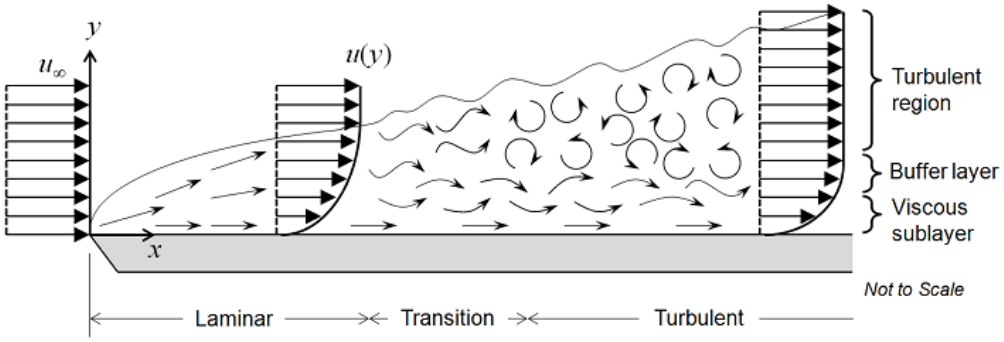

Figure 4 A visualization of the different sub-layers and states of the flow over a wall **(Frei, 2014)**.

The distance from the wall to the end of the buffer layer is defined as δ and is visualized in Figure 5. Thereafter the turbulent region extends to approximately 100δ after which the log-law is valid and the free-stream region with inviscid flow begins. Free-stream means that the wall shear stress does not affect the velocity profile.

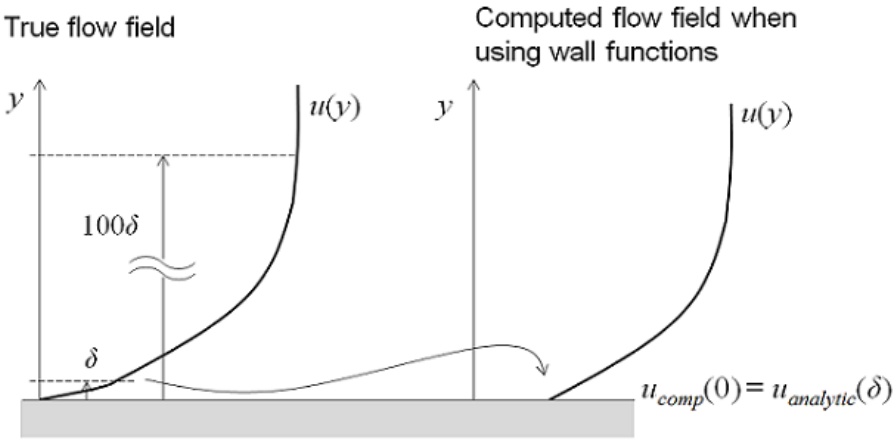

Figure 5 The difference between a flow field using wall functions and a true flow field **(Frei, 2014)**.

RANS can be used to compute the flow in all four regions though it may be advantageous to approximate the viscous and buffer layers with wall functions. Wall functions are used to approximate the flow field in the viscous and buffer regions by setting a non-zero velocity at the wall. This means that these regions are not simulated which results in less computational time but lower accuracy of the final result. If a higher accuracy is desired a full turbulence model is applied. There are several RANS turbulence models that use wall functions in

different ways but they all use Navier-Stokes equations with an added turbulent viscosity term.

A turbulence model available in STARCCM+ is the k-ε model in which the two variables k (turbulent kinetic energy) and ε (rate of dissipation of kinetic energy) are solved for. This model is advantageous as it shows good convergence rates for low memory use. A variant of the k- ε model is the realizable k- ε model which is used in this project. In order to use this turbulence model efficiently, a boundary layer mesh is created in which the mesh closest to the wall is composed of shallow rectangles or triangles to match the velocity change normal to the wall. However, in order for this turbulence model to work the normalized height (y^+) of the cell closest to the wall should be approximately equal to or larger than δ. If the cell is less than δ there is a risk that the simulation will crash and not converge. (Frei, 2014)

3. Methodology

The methodology chapter first discusses the computational models used in this study and then dissects the flowchart in Figure 2 part by part in chronological order.

3.1. The Computational model

There are two main computational models used in this study, one BH model and one waterjet SP model. Both models are constructed according to the method described in *Waterjet Propeller Hull Transom Clearance* (Eslamdoost, et al., 2013). In short, the Finite Volume method is used to solve mass and momentum conservation equations. This method in combination with the Volume of Fluid method to obtain volume fraction of liquid, and the standard realizable k- ε turbulence model with wall functions, gives the system of equations which needs to be solved. Due to symmetry, half of the hull is simulated in order to reduce CPU hours.

For each simulation there are some initial parameters which need to be specified: the position of the LCG determining the initial trim, the wind and current velocity, the towing force, the rope force and the waterjet thrust vector. For BH simulations the towing force is added at the point in which the model was towed during towing tank tests. For SP simulations a rope force is added which compensates for the increased viscous resistance due to scaling effects. In this study the rope force is set to a constant value of 4.6 Newton corresponding to the rope force for the design Froude number (F_n=1). This is done since the magnitude of resistance is in this study considered of less importance than the overall resistance trends. Another parameter specified in SP is the waterjet thrust vector positioned at the nozzle exit. Modelling the propulsion system is done by using the geometry of the waterjet and replacing the impeller geometry with a body force distributed inside its volume.

3.2. Grid dependence study

The grid dependence study aims at finding the most efficient mesh for BH regarding numerical uncertainty versus computation time, for the lowest Froude number that will be simulated in this project. An efficient mesh for SP has been developed by Arash Eslamdoost, why only a grid dependence study for BH is carried out. The reason for choosing the lowest Froude number is that the wave frequency along the hull is higher for lower Froude numbers which as a result requires a finer mesh to describe the flow field. This mesh configuration can therefore be applied for higher Froude numbers by assuming that the numerical uncertainty will not increase. It should be noted that the grid dependence study is carried out for fixed hull because the theory for grid dependence studies is well developed only for a time independent flow.

The first step in the grid dependence study is to determine the base size and primary mesh for the computational domain. The idea behind base size in STAR-CCM+ is that other values like surface minimum/target size, boundary layer thickness are set proportionally to the base value. So if the mesh is to be refined or coarsened the base size value is adjusted and all other values which are defined by the ratio to the base size will change automatically.

The second step is to set the grid refinement ratio which determines the percentage change of each cell in every direction for the entire grid. A rule of thumb for setting the refinement ratio is that it should not exceed $\sqrt[4]{2}$. For this study the refinement ratio is 15% and is applied to the base size. In this case there are certain parts of the hull that have a larger and smaller influence on the resistance than others such as the boundary layer (finer grid) and deck (coarser grid) respectively. Therefore the mesh at these regions are manually determined and do not follow the refinement ratio.

Six meshes are generated with increasing number of cells and the simulations are started. The simulations continue until they reach convergence for a certain output parameter, in this case the total hull resistance. The mean values of total hull resistance are implemented in a Matlab code which uses the LSRM to calculate the *p*-value and the numerical uncertainty (U_{SN}). The numerical uncertainties for the different meshes are compared to the computational time used to reach convergence and out of this an ideal mesh is chosen.

3.3. Variation study

The variation studies apply the previously determined effective mesh for BH from the grid dependence study and the SP mesh from Arash. Using these meshes for simulations in two degrees of freedom (free sinkage & trim) and comparing the results to measured data, validations can be carried out and thrust deductions calculated.

3.3.1.Variation of Froude number

The main purpose of the variation of Froude number study is to validate the computational model for BH and to find out the effect of transom clearance on thrust deduction for an initial bow up trim of four degrees. The Froude number for which this occurs is denoted the critical Froude number (c.a. 0.5). Therefore a span of Froude numbers around the critical Froude number is investigated. The reason for choosing a four degree bow up trim is to see the effect on the transom clearance phenomena for an extreme case. Thirteen simulations for BH and seven for SP are run and out of these simulations resistance peak and trim plots are created for further comparisons.

3.3.2. Variation of initial trim

Four simulations each for BH and SP are run at four initial trims. The four initial trims are determined in STAR-CCM+ by setting both the angle of the computational domain and the position of the longitudinal center of gravity (LCG) that corresponds to the initial trim angle at zero speed. Resistance and T_{net} curves are created for BH and SP respectively for further comparisons.

3.3.3. Variation of waterjet intake position

The systematic variation study requires hull geometries with the waterjet mounted at five different positions along the hull. These five positions require a unique interface design of the waterjet intake due to the geometrical changes of the hull. The waterjet geometries are generated with in-house software made by Rolls-Royce called Propcalc. The geometries

include a waterjet housing, inlet, nozzle, impeller and shaft. To adjust the longitudinal position of each waterjet intake, the piping from the intake to the pump is extended or shortened. The position of the pump is always the same, mounted on the inside of the transom.

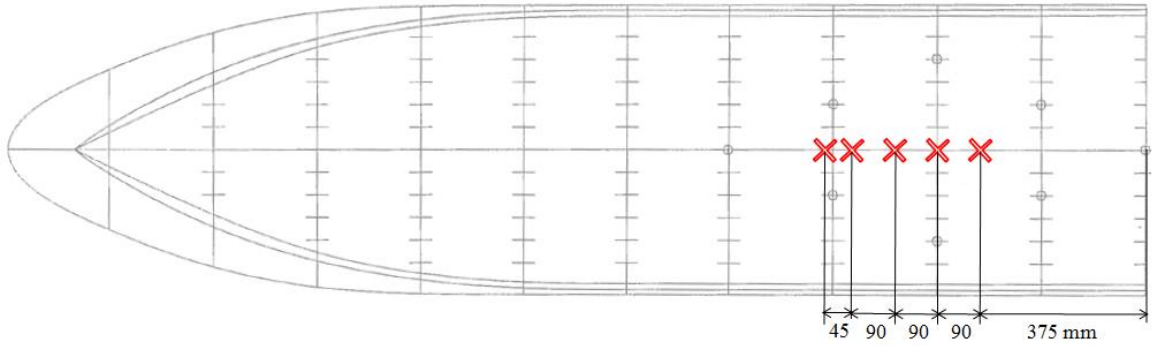

Figure 6 The five waterjet intake positions from stern (Pos 0) to bow (Pos 4) of the STREAMLINE hull.

The positioning span of the waterjet is limited for practical reasons from position 0 at 375 mm to position 4 at 645 mm measured from the transom. This limit is due to the geometrical complexity of the hull further towards the bow which would introduce problems in Propcalc. The red crosses in Figure 6 represent the centers of the waterjet intakes. The positions of the intakes are varied with the pump outlet diameter (D=90 mm) as a reference length.

The SP simulations are run for these positions of the waterjet intake against four Froude numbers. These Froude numbers are also simulated for BH in order to be able to measure the thrust deduction fraction. The results are presented in thrust deduction fraction and T_{net} against waterjet intake position and Froude number.

3.4. Validation study

The process for a complete validation is described in the theory chapter. However, a complete validation of the computational models is not possible. The issue in the validation process is the missing experimental uncertainty (U_D) that is used to determine the total validation uncertainty (U_{val}). This experimental uncertainty is a sum of all the inaccuracies affecting the experimental measurements and is calculated by the test facility. SSPA has not disclosed this uncertainty for their model tests. Instead of a complete validation, error trends between test and simulation data are calculated for BH and SP to get a perception of the reliability of the models. This is done for the Froude number variation and initial trim studies.

4. Results & Discussion

The results for each study are presented and discussed in this chapter. The results from the validations are discussed in combination with the variation studies and not in a separate chapter.

4.1. Grid dependence study

Study	Input	Output
Grid dependence study	- 6 mesh sizes btw 10^6- 10^7 cells - F_n = 0.398 - BH, fixed hull - Even keel	- Efficient mesh size for BH

Figure 7 shows a graph of the convergence of the measured hull resistance for the five converged meshes. The base size on the x-axis decreases with a 15% refinement ratio for each mesh point.

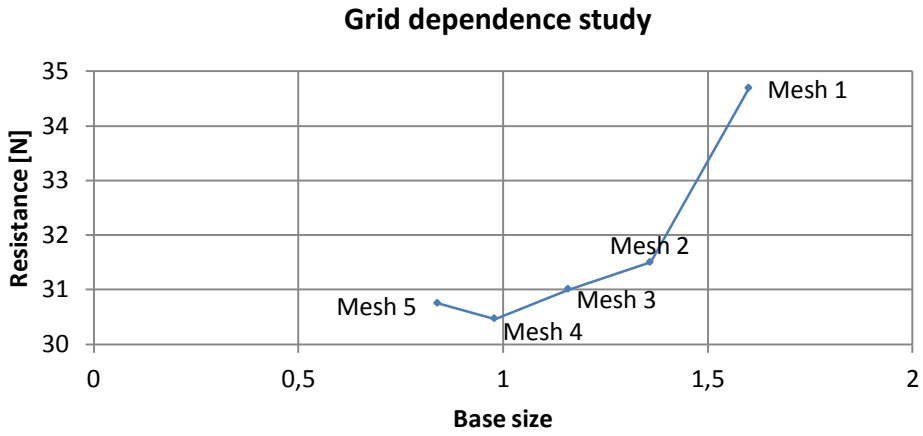

Figure 7 Graph over the different meshes tested for BH in the grid dependence study.

The effective mesh size is the third mesh which has a small enough numerical uncertainty compared to the convergence time. The numerical uncertainty is calculated using a Matlab code based on the Least Square Root Method mentioned in chapter 2. One can see in Table 3 that mesh 4 requires twice as much convergence time for a slight change in resistance coefficient and a slightly smaller numerical uncertainty. The sixth mesh was running for 67 hours on six nodes without reaching any convergence. This may be due to that the cell closest to the hull is smaller than δ meaning that the wall function is not satisfied. The wall function's approximation of the viscous and buffer sub-layers, at a non-dimensionalized length ($y^+ = \delta$) from the hull, should be described by one cell length.

Table 3 The total result of the grid dependence study. The row highlighted with green is considered as the most efficient mesh for BH.

Mesh nr.	Number of elements	Resistance coefficient (C_T) [10^{-3}]	Numerical Uncertainty (U_{SN}) [10^{-4}]	Convergence time (Node hours)
1	1044694	15,2	55.728	16
2	1706204	13,8	13.140	36
3	2592960	13,5	4.316	80
4	4253628	13,3	1.667	158
5	6484700	13,4	1.126	175
6	10771065	No convergence	No convergence	-

4.2. Variation of Froude number

Study	Input	Output
Variation of Froude number	- 13 F_n around $F_{n,critical}$ for BH - 7 F_n around $F_{n,critical}$ for Self prop. - initial trim (LCG)= Bow up (4˚) - Free sinkage & trim	- Resistance and T_{net} + trim data for BH and SP respectively at constant initial trim (LCG) - Thrust deduction fraction

The total resistance coefficient curves from the simulated and measured data for BH are plotted in Figure 8. The resistance peaks appear at different Froude numbers but at approximately the same magnitude. Since the trends of the curves are similar but shifted, the computational model for BH gives an indication of being reliable. The error trend converges against an error of 6-8% after the measured resistance peak. Since the error trend does stabilize after the measured resistance peak, the computational model appears to become more reliable for higher Froude numbers.

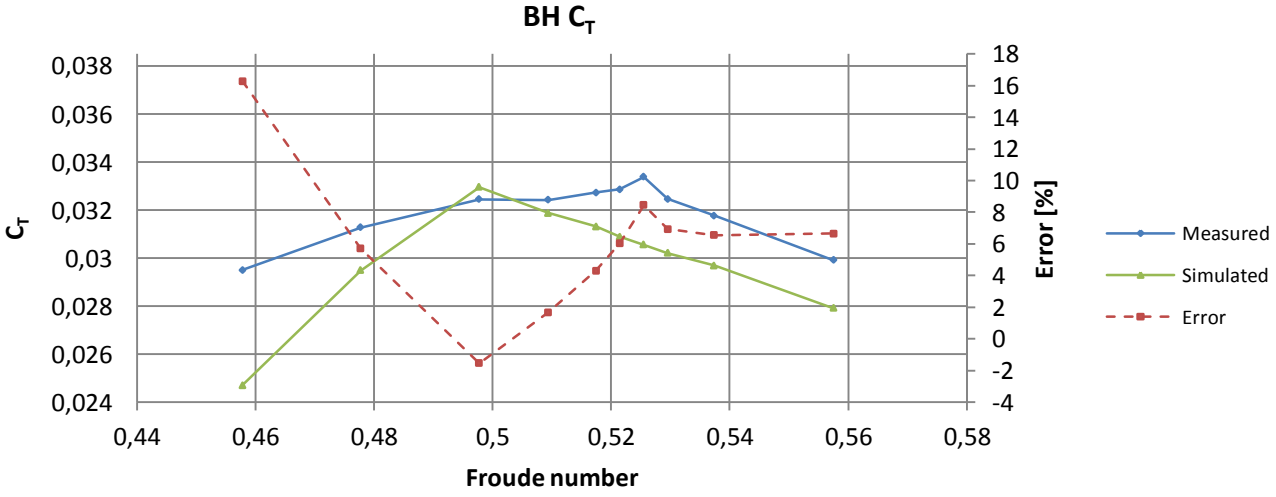

Figure 8 A comparison of the total resistance coefficient between the measured and simulated model. The simulated resistance peak appears at Fn=0.498 and the measured at Fn=0.526.

As mentioned in the previous work chapter, the paper *Waterjet Propelled Hull Transom Clearance* (Eslamdoost, et al., 2013) shows two main conclusions. The first conclusion is that the correspondence between measured BH and simulated BH data is better for Froude

numbers after the measured resistance peak. The second conclusion from his paper is that there is a difference in resistance peak between SP and BH for even keel trim and that the resistance peak corresponds to the transom clearance.

The first conclusion is also shown to be the case for this bow up initial trim since the simulated resistance follows the trends of the measured data after the peak. Before the peak the trends do not match giving an error span of 5-16 % before the simulated peak. The reason for this is unclear and the source of the error is hard to determine. It may be due to the difficulty in measuring the resistance for low Froude numbers just before the peak because of the transient, i.e. time dependent flow at the transom. The complexity of the flow may also cause over or under predicted resistance for the simulations. The flow at the transom for Froude numbers just before and after the simulated peak is shown in Figure 9. The figures display velocity vectors of the flow at the transom where one can see that the flow has higher complexity before the resistance peak due to backflow against the transom which does not appear after the resistance peak when the transom is dry. The backflow and complexity makes the resistance harder to measure and simulate than when the flow is straight and homogeneous.

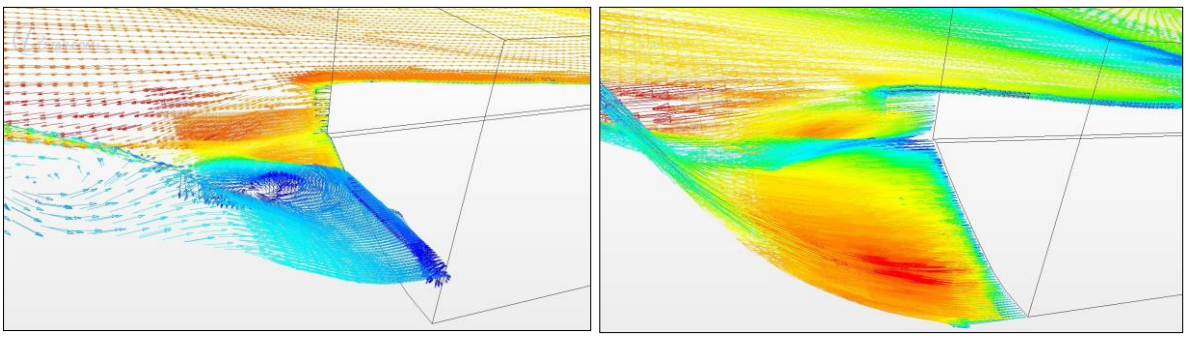

Figure 9 The picture to the left shows the complex flow at the wetted transom for BH before the resistance peak at Fn=0.478. The picture to the right shows a more predictable flow field at the transom for BH after the resistance peak at Fn=0.509. The colored arrows in the pictures represent velocity vectors where the red color is high velocity and blue is slow velocity.

The second conclusion is also shown to be the case also for this bow up initial trim as seen in Figure 10. The reasons for the difference in resistance peaks are most probably occurring due to the reasons explained in his paper and a short summary of the reasoning is given in chapter 1.2. It should be pointed out that in order to get a more exact value for the critical Froude number, more simulations need to be run for Froude numbers around the peak. The rightmost transoms in Figure 10 show that the transom is clear, however it is not certain that these Froude numbers are the exact lowest Froude numbers in which the resistance peaks appear.

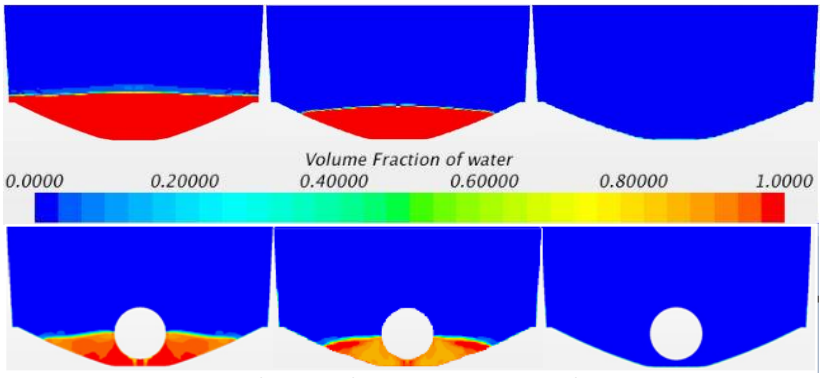

Figure 10 The upper row displays the volume fraction of water on the transom for BH at Fn= 0.458, 0.478, 0.498 respectively. The lower row displays the volume fraction of water on the transom for SP at Fn= 0.415, 0.4344, 0.458 respectively.

The trim angle data from the computational model for SP is compared with the trim data from SSPA for four degrees initial trim in Figure 11. The figure shows that the correspondence between simulated and measured data is good and the trends are similar. All measured trim data points fall within a three percent error margin. However, with only four data points from model tests, it is hard to say if the computational model is indeed valid.

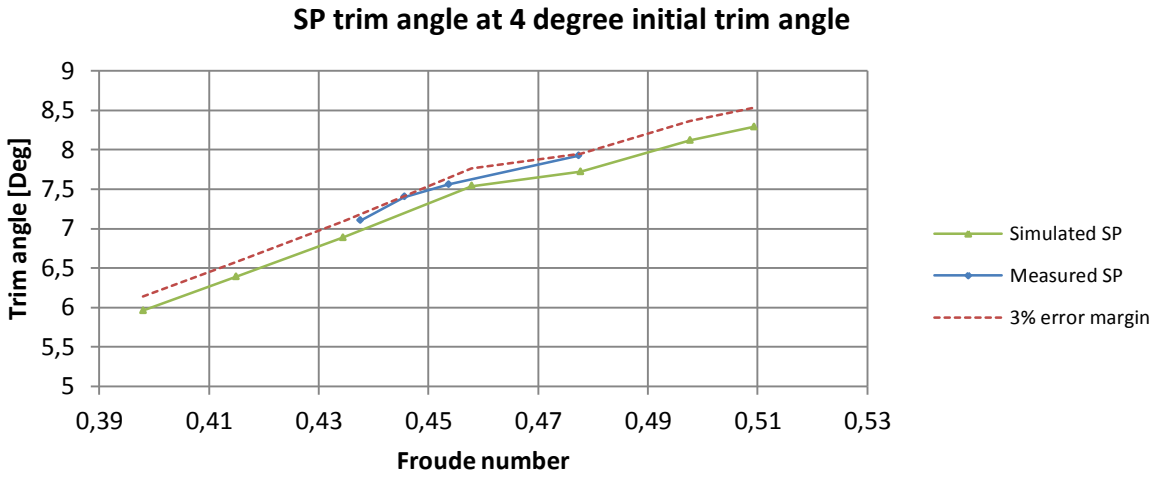

Figure 11 A comparison between trim angles for the simulated and measured SP model.

The comparison between total resistance coefficients for BH and SP in Figure 12 shows that the resistance for SP is higher for these low Froude numbers. This entails a positive thrust deduction fraction for all these Froude numbers shown in Figure 13.

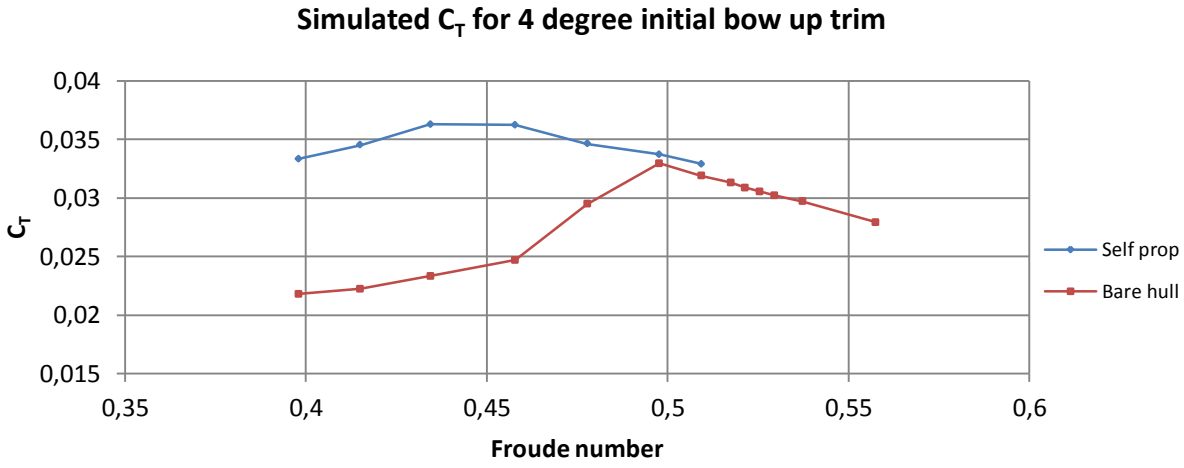

Figure 12 The difference in total resistance coefficient (C_T) between simulated SP and BH.

According to experience it is expected to have a positive thrust deduction fraction before the SP peak and this statement is backed up by simulations carried out by Arash Eslamdoost shown in Figure 1.

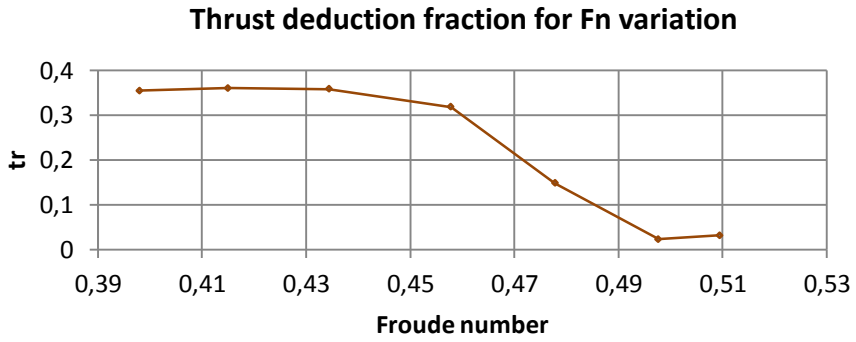

Figure 13 The thrust deduction fraction around the resistance peaks.

4.3. Variation of initial trim

Study	Input	Output
Variation of initial trim	- F_n = 0.996 - initial trim = 0.786˚, 0˚, -0.819˚, -1.693˚ - BH & SP, free sinkage & trim	- Resistance and T_{net} + trim data for BH and SP respectively at constant F_n - Thrust deduction fraction

The resistance curve from the simulation for BH follows the trend from the measured resistance data with an error between 6-8% as seen in Figure 14. This gives an indication that the model is reliable in terms of overall trend. As seen from the variation of Froude number study, the error span converged to between 6-8 % for the higher Froude numbers for BH. The error span is the same in this case for Froude number 0.996 for all four initial trims. This gives an additional indication that the BH model is valid also for these initial trims and for higher Froude numbers.

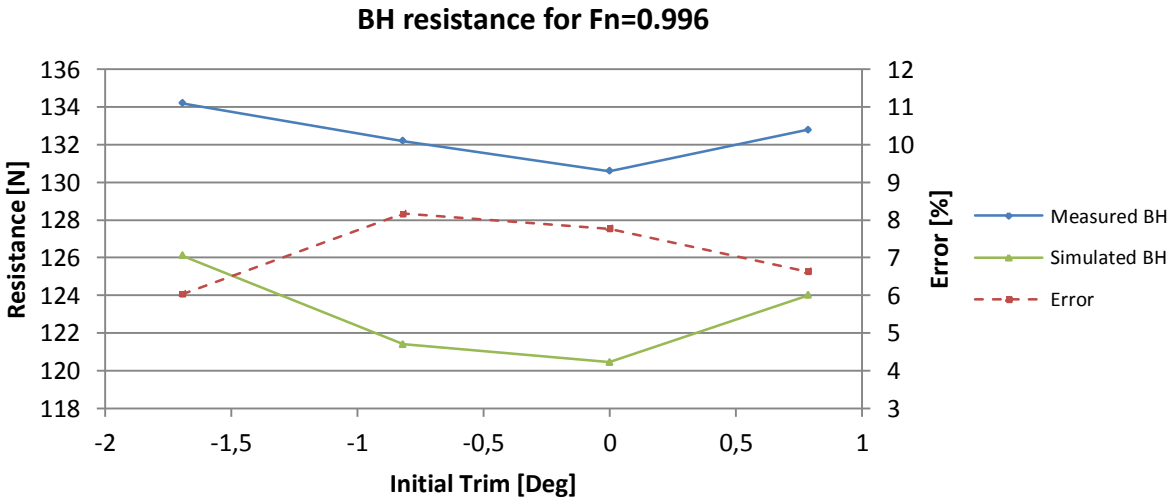

Figure 14 A comparison between measured and simulated resistance for BH.

There is not enough available test data to generate an error trend for SP for this trim variation study. This means that the validity of the SP model cannot be checked using trim variation. Even so, when comparing the SP and BH simulations one can see that the resistance is larger at bow up trims for BH compared to SP. For bow down trims the SP increases more in resistance compared to BH. The optimum initial trim for this hull at design speed is the even

keel trim with LCG at 0.9 meters from the transom. This result is found both from the SP and BH data.

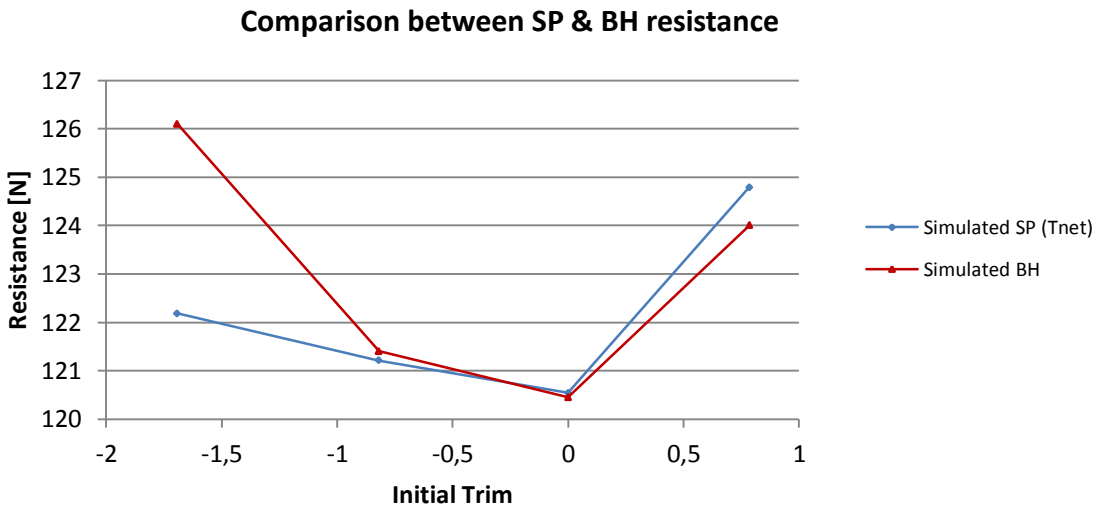

Figure 15 The difference in resistance between BH and SP for various initial trim and constant Fn=0.996.

Looking at the thrust deduction fraction curve in Figure 16 one can see that the values for thrust deduction fraction are reasonable according to experience. The largest thrust deduction fraction is slightly more than 3% for a bow down trim of -1.693 degrees. The trend is that thrust deduction increases with increased bow down trim.

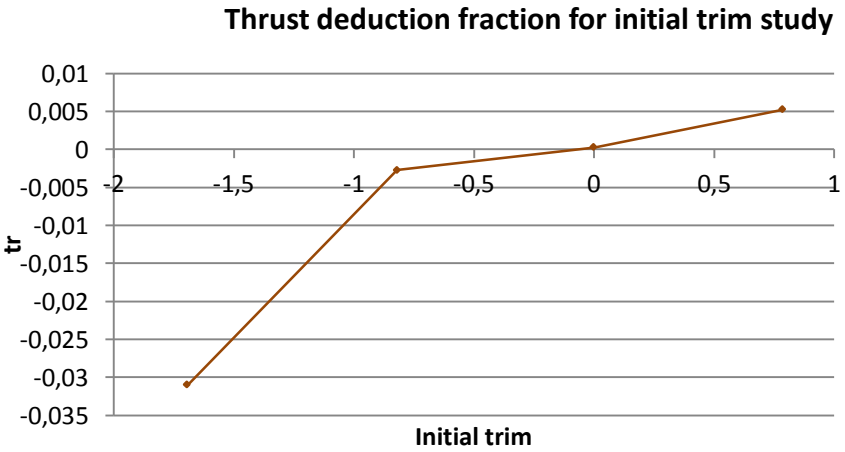

Figure 16 The thrust deduction fraction for Fn=0.996 at various initial trims.

4.4. Variation of waterjet intake position

Study	Input	Output
Variation of waterjet intake position	-Five intake positions -F_n=0.398, 0.498, 0.697, 0.996 -BH & SP -even keel -free sinkage & trim	- Resistance and T_{net} data for BH and self propulsion respectively for varying F_n and waterjet intake position - Thrust deduction fraction

The results from this study are shown in Figure 17 and Table 4. As can be seen, the position of the waterjet intake has an impact on the resistance for all of the Froude numbers tested. Position 1 is shown to be the most efficient position, with a resistance of between 2-6% lower than the largest resistance for each respective Froude number.

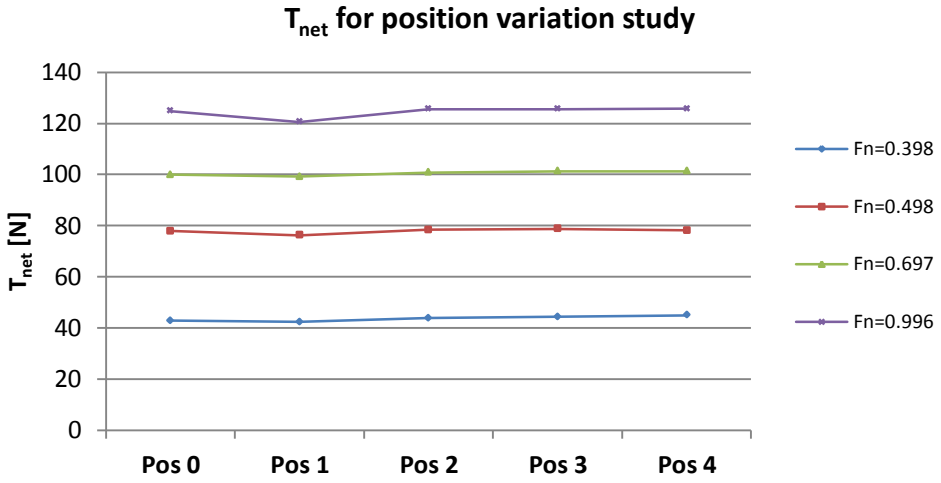

Figure 17 The longitudinal component of the thrust vector $\boldsymbol{T_{net}}$ vs waterjet intake positions for four different Fn.

This can be clairified by row number two for position 1 in Table 4 . This row contains the lowest T_{net} values for each Froude number.

Table 4 The corresponding $\boldsymbol{T_{net}}$ data to Figure 17 in Newton.

	Fn=0.398	Fn=0.498	Fn=0.697	Fn=0.996
Pos 0	42,77	77,87	99,87	124,91
Pos 1	42,39	76,21	99,15	120,54
Pos 2	43,84	78,33	100,8	125,6
Pos 3	44,38	78,75	101,25	125,56
Pos 4	44,98	78,19	101,36	125,77
BH	31,34	73,15	94,38	120,45

Figure 18 shows that the thrust deduction fraction for the STREAMLINE hull decreases with increased Froude number. The lowest thrust deduction fraction is found for position one for Fn=0.996.

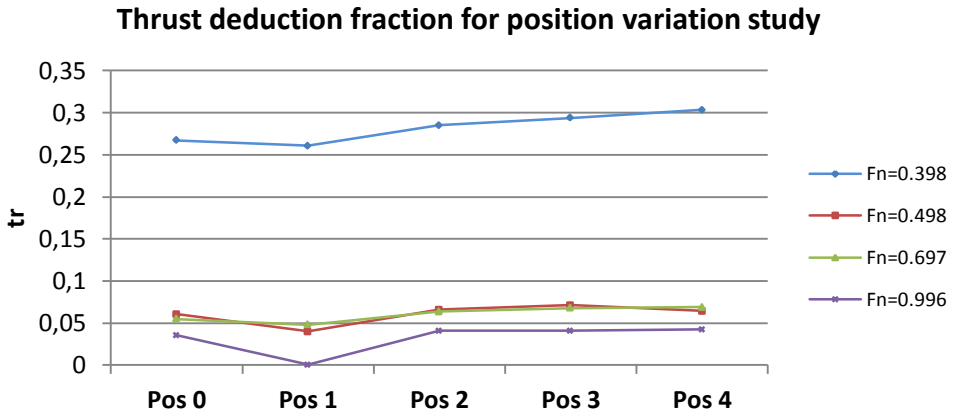

Figure 18 The thrust deduction fraction for the various waterjet intake positions and Froude numbers.

The change in the slope of the curve in Figure 19 shows the rate of decreasing thrust deduction fraction for each Froude number at Pos 1. It is interesting to note that the slope between Fn=0.398 and Fn=0.498, i.e. the first two points on the curve, is much steeper than the slopes after Fn=0.498. It seems that the rate of decreasing thrust deduction fraction is much lower after the critical Froude numbers.

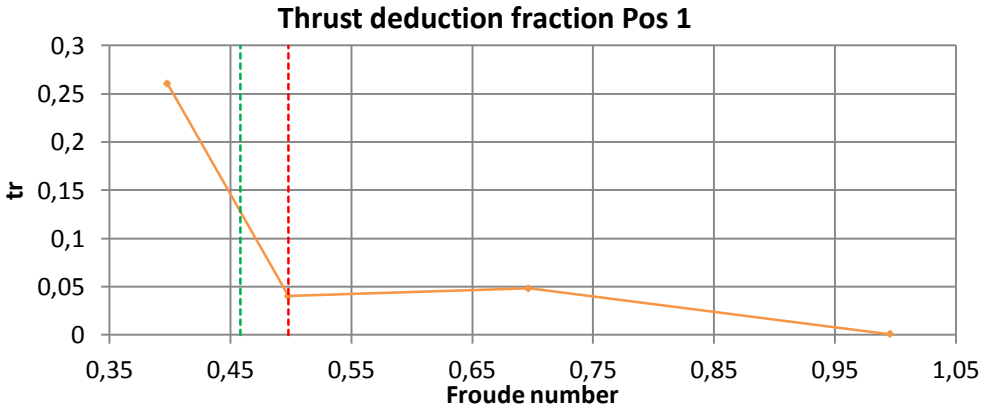

Figure 19 The orange line represents the thrust deduction fraction for the waterjet intake at position one at Fn=0.996. The green and red dotted lines are the critical Froude numbers for SP and BH respectively.

When generating the waterjet geometries for the different positions only the length of the pipe from the intake to the pump is altered, together with the interface between the intake and the hull. By increasing the length of the piping the displacement of the hull increases due to the added mass of the water inside the pipe. This added displacement is not accounted for in the simulations. A quick calculation shows that the added weight for increasing the pipe length with one reference length (D=90 mm) is 0.7%. The total effects of this added displacement should be studied by adding this effect to the computational model.

5. Conclusions

The grid dependence study results in an effective mesh size for the BH computational model of around 2.6 million elements. The BH model has been validated using error trends from the different parameter studies. Since the trends of the curves are similar but the peaks are shifted in the Froude number variation study (Figure 8), the computational model for BH gives an indication of being reliable. The error trend converges against a stabilized error between 6-8% after the measured resistance peak. This same error span appears from the trim variation study (Figure 14) suggesting that the BH model becomes reliable for higher Froude numbers after the measured resistance peak.

The computational model for SP from the studies carried out by Arash Eslamdoost has been used to run the SP simulations in this project for free sinkage and trim. Due to a lack of model test data for SP, a thorough validation has not been possible. However, with the four model test data points available it seems that the SP model is reliable at least within this short Froude number span (Figure 11). Also, the plot of the total resistance coefficient from the Froude number variation study (Figure 12) shows reasonable results for the SP model in respect to experience and similarities to the study carried out by Arash Eslamdoost, displayed in Figure 1. Finally, the thrust deduction fractions from the trim variation study (Figure 16) are within a reasonable span and the largest negative thrust deduction fraction found is about -3% for bow up trim of -1.693 degrees.

The Froude number variation study shows that the transom clearance phenomena for a four degree initial bow up trim coincides with the resistance peaks for BH and SP. It also shows that the resistance peak for SP appears at a lower Fn than the resistance peak for BH. These are the same conclusions as reached by Arash Eslamdoost for even keel initial trim.

From the trim variation study, it is found that the most optimum initial trim at design Fn for the STREAMLINE hull is even keel (zero degrees). The resistance increases for both bow up and bow down trims at this velocity, see Figure 15.

From the position variation study at even keel initial trim it seems that the position of the waterjet intake within the tested span has an effect on the resistance as shown in Figure 17. It is clear that position 1 gives a 2-6% lower resistance for every Froude number tested. This means that the impact of the longitudinal position of the waterjet intake relative to the impact of initial trim and velocity is small. If a 2-6% decrease in the resistance is considered to be significant for its application, from an efficiency and sustainability point of view, then the intakes position is of importance. But, if this decrease is considered to be insignificant then the intake can be placed where it is most suitable from another perspective such as general arrangement. If the results from the position variation study can be generalized to other initial trims, Froude number spans, hull shapes and a larger position span, then Rolls Royce have the possibility to place the waterjet unit at different positions without largely affecting the total resistance of the hull.

6. Future work

The most important step in a continuation of this study is to gather more model test data for SP so that a validation such as for BH can be carried out. In the case of BH, error spans were found for the Froude number variation study and trim variation study. It would be preferable to minimize these error spans for BH simulations in order to not accumulate these errors to the SP model. This can be done by thoroughly investigating the reasons behind the shift in resistance peak between the measured and simulated BH data and also by investigating the difference in the magnitude of resistance from the trim variation study.

When the error spans have been minimized and the SP model validated, the position variation study should be expanded to see if the trends for the STREAMLINE hull continue when the parameters are changed. The span of Froude numbers need to continue above the design Froude number and simulations should be carried out for different bow up and bow down initial trim angles. Similar position variation studies should be carried out to see if the trends and results can be generalized for other hull shapes and waterjet configurations. For example, hulls with larger or smaller L/B - ratios, catamarans and dual waterjet configurations. It should also be investigated why position 1 is the most efficient position and why all the other positions result in similar resistance for the tested Froude numbers.

As mentioned in the methodology chapter, the rope force was set to a constant value for all Froude numbers. In future studies the simulations should be run with calculated rope force values for each Froude number in order to more accurately account for viscous effects. Calculating specific rope forces for different Froude numbers can be done using a calculation procedure from the International Towing Tank Committee (ITTC). The procedure is shown below.

$$R_a = \frac{1}{2}\rho_m S_m V_m^2 [C_{Fm} - (C_{Fs} + \Delta C_F)] \quad (32)$$

where

R_a = rope force [N]
ρ_m = mass density of tank water [Ns^2/m^4]
S_m = wetted surface [m^2]
V_m = speed [m/s]
C_{Fm} and C_{Fs} = frictional resistance coefficients (ITTC 1957)
ΔC_F = friction correction dependent on surface condition of the ship hull (Normally $\Delta C_F = 0.0004$)

$$C_F = \frac{0.075}{(\log_{10} R_n - 2)^2} \quad where \quad R_n = \frac{VL}{\nu} \quad (33)$$

where

V = speed [m/s]
L = length of waterline for ship and model respectively [m]
ν = kinematic viscosity [m^2/s] (ITTC 1960)

The rope force for Froude number 0.398 has in this study been calculated and simulated as a test to see the effect on the magnitude of resistance. This test showed a decrease in resistance of about 1.5-2%.

As mentioned in the result chapter, the added displacement due to the added mass of water inside the pipe is not accounted for in the simulations. The total effects of this added displacement should be studied by adding this effect in order to get a more accurate model.

7. References

Eslamdoost, A., 2012. *Investigations of Waterjet/Hull Interaction Effects,* Göteborg: Department of Shipping and Marine Technology.

Eslamdoost, A., Larsson, L. & Bensow, R., 2013. *Waterjet Propelled Hull Transom Clearance.* Mülheim/Germany, s.n.

Frei, W., 2014. *blog Comsol.* [Online]
Available at: http://www.comsol.com/blogs/which-turbulence-model-should-choose-cfd-application/

Larsson, L. & Raven, H. C., 2010. *The Principles of Naval Architecture series, Ship Resistance and Flow.* New Jersey: The Society of Naval Architects and Marine Engineers.

Schneekluth & Bertram V, H., 1998. Ship Design for Efficiency and Economy (2nd Edition). In: *Ship Design for Efficiency and Economy (2nd Edition).* Oxford: Butterworth-Heinemann, pp. 180-183.

Zou, L., 2012. *CFD Predictions Including Verification and Validation of Hydrodynamic forces and Moments on Ships in Restricted Waters,* Göteborg: Department of Shipping and Marine Technology.